Contents lists available at ScienceDirect

International Journal of Biological Macromolecules

Lactobacillus delbrueckii subsp. *bulgaricus* derivatives for 3D printed alginate/hyaluronic acid self-crosslinking hydrogels: Manufacturing and wound healing potential

Giulia Remaggi [a], Benedetta Bottari [a], Elena Bancalari [a], Ovidio Catanzano [b], Erasmo Neviani [a], Lisa Elviri [a,*]

[a] *Department of Food and Drug Science, University of Parma, Parco Area delle Scienze 27/A, 43124 Parma, Italy*
[b] *Institute for Polymers, Composites and Biomaterials (IPCB-CNR), Via Campi Flegrei 34, 80078 Pozzuoli, NA, Italy*

ARTICLE INFO

ABSTRACT

Derivatives [i.e. proteins and exopolysaccharides (EPS)] from *Lactobacillus delbrueckii* subsp. *bulgaricus* (LB) were extracted, characterized, and for the first time used in the production of novel self-crosslinking 3D printed alginate/hyaluronic acid (ALG/HA) hydrogels, as high-value functional biomaterials with therapeutic potentials in regenerative medicine applications. Derivatives coming from two different LB strains, LB1865 and LB1932, were tested in-vitro and compared for their cytotoxicity and effect on proliferation and migration on human fibroblast. EPS received particular attention as showing relevant dose-dependent cytocompatibility against the human fibroblast. The derivatives showed an ability to increase cell proliferation and migration, quantifiable between 10 and 20 % if compared to controls, with higher values for the derivatives obtained from the LB1932 strain. These were explained by liquid chromatography-mass spectrometry targeted protein biomarker analysis as a decrease in matrix-degrading and proapoptotic proteins, associated with an increase in collagen and anti-apoptotic proteins production. LB1932 enriched hydrogel was found to be of benefit compared to control dressings, giving the more promising results as potential for in vivo skin wound healing tests.

1. Introduction

Tissue engineering is an interdisciplinary field of study, which aims to develop active materials capable of recreating, repairing, or engineer tissues and organs [1]. In this context, the development and application of innovative biomaterials as advanced therapeutic solutions are constantly evolving [2]. One of the application fields of tissue engineering deals with wound healing, a complex biological process including inflammation, proliferation, and tissue remodeling. The wound healing process consists in the activation of numerous and still poorly understood intracellular and intercellular pathways able to restore the complex physiological integrity and functionality of these multilayer tissues [3]. Wound healing is a global and serious medical issue requiring for more effective and cost-effective dressings [4]. Among the most promising strategies, the use of bacteria, both through oral and topical administration, has been recently considered, with good results achieved in cutaneous wounds healing [5–11]. Selected bacteria demonstrated stimulatory effects on wound repair activating

lymphocytes and macrophages, favoring immune system activities, inhibiting inflammation and promoting cell proliferation. Species of lactic acid bacteria (LAB) have been identified as promoters of the wound healing process. LAB have a long history of safe exploitation by humans, being used for centuries in food production and preservation and as probiotic agents to promote human health [12,13]. LAB have been classified as food grade microorganisms [generally recognized as safe (GRAS) organisms by the US Food and Drug Administration (FDA)] and fulfill criteria of the qualified presumption of safety (QPS) according to the European Food Safety Authority [14]. Due to their metabolisms and their health improving effects, LAB plays important roles in food, dairy, agricultural, pharmaceutical, and medical applications [15]. Their potential benefit in tissue regeneration processes has been demonstrated using both whole living bacteria and/or some of their derivatives. For example, *Lactobacillus delbrueckii bulgaricus* (LB) and *Lactiplantibacillus plantarum* whole cells improved diabetic wound healing via regulation of inflammatory factors [8]; soluble fraction from lysates of *Streptococcus thermophilus*, *L. plantarum*, and *Lactobacillus*

---

* Corresponding author at: Parco Area delle Scienze 27/A, 43124 Parma, Italy.
  E-mail address: lisa.elviri@unipr.it (L. Elviri).

acidophilus promoted the in vitro re-epithelialization of HaCaT scratched monolayer through a mechanism involving nitric oxide synthase 2 [16]. Furthermore, exopolysaccharides (EPS) produced by some lactobacilli could favor fibroblast regenerative processes [17], by inducing fibroblasts migration and exhibiting an anti-elastase and anti-collagenase potential on human fibroblast. EPS could also contain residues of D-glucuronic acid, a fundamental component of the hyaluronic acid normally presents in the extracellular matrix (ECM), involved in the mechanoperception of cells [17].

In the last few years, advanced therapies able to mimic the ECM and thus cell adhesion, migration, and proliferation were developed. Three-dimensional (3D) scaffolds have been successfully involved in wound healing as supports for cell growth, maintenance and differentiation thanks to their suitable structural, physical and biochemical characteristics [1,2]. Nowadays 3D printing can be considered the main technology utilized in scaffold production for tissue engineering purposes [18]. Numerous advantages over traditional manufacturing methods, such as the possibility to design complex 3D multi-layered structures with tunable features and most importantly, device personalization have been well demonstrated [19–22]. These are key points in the development of advanced release systems with ad hoc features such as personalized locally controlled drug release [23]. Among the materials used as inks for 3D printing, natural polymers are certainly some of the most studied, as they can promote adhesion and provide support for cell growth. In particular, natural-based 3D printed hydrogels presents favorable biomimetic environments for living cells, such as high-water content, tunable mechanical properties and degradation rates, porous structure and the possibility to incorporate bioactive molecules or living cells [24–27]. Moreover, they are also biodegradable and therefore can be progressively degraded and replaced by a new extracellular matrix in tissue regeneration processes [28,29].

One of the most used biopolymers to prepare hydrogels for biomedical applications is alginate (ALG), due to its characteristics of biodegradability, non-toxicity and non-immunogenicity [30]. ALG is a natural polysaccharide used for the production of hydrogels by the addition of divalent soluble cations (such as Ca^{2+}, Ba^{2+}, Zn^{2+} or Sr^{2+}) [31]. The internal gelation of the ALG through calcium carbonate and δ-glucono-lactone ($CaCO_3$ – GDL) system can be a useful crosslinking technique to obtain homogeneous hydrogels thanks to a slow and controlled release of calcium ions. The homogeneous hydrogels thus obtained, usually present a well-defined porosity, uniform mechanical properties and the possibility of including water-soluble active ingredients in the formulation [31,32]. To date, the use of self-crosslinking alginate-based inks for 3D printing is still in its infancy [33], but the ability of the internal gelation to prepare 3D homogeneous hydrogels open many possibilities [34]. The combination of ALG with other biopolymers such as hyaluronic acid (HA) is of particular interest. HA is a natural nonsulfated linear glycosaminoglycan, biodegradable and non-immunogenic [35]; it is successfully used for hydrogels or nanoparticles production in regenerative medicine or drug delivery purposes [36,37] High molecular weight HA (>100 kDa) is a polymer widely represented in a large variety of tissues, constituting one of the main components of the extracellular matrix. It contributes to the hydrodynamic regulation of tissues, cell compression and processes such as inflammation and tissue regeneration. In the early stages of wound healing, HA provides temporary support for the transport of nutrients and waste products, while promoting the migration and proliferation of keratinocytes. Moreover, evidence of HA mediated modulation of fibroblast gene expression involved in repair and remodeling of extracellular matrix have been reported [38,39].

In this whole frame, since the wound healing process involves many variables and collective biological mechanisms, a reliable understanding of the therapeutic efficacy of natural derivatives is still a big challenge.

This work aims to add insights into this field, through different steps: 1) to extract and characterize derivatives from two different L. *bulgaricus* (LB) strains; 2) to develop innovative self-crosslinking inks for 3D printing extrusion technology based on ALG, ALG/HA and ALG/HA/LB derivatives mixtures; 3) to manufacture novel 3D printed active ALG/HA hydrogels containing the characterized LB hydrophilic derivatives to be applied in regenerative medicine applications; 4) to perform a series of in-vitro tests on human fibroblasts to investigate the potential capability of the manufactured hydrogels in wound healing.

2. Materials and methods

2.1. Materials

2.1.1. Reagents

Sodium alginate (Ph. Eur. grade; molecular weight by gel filtration chromatography (GFC) 180–300 kDa; slowly soluble in water), urea, and calcium carbonate ($CaCO_3$) were purchased from Carlo Erba (Carlo Erba Spa, Milan, Italy). Hyaluronic acid [Halien, High MW 100–1000 kDa (GFC)], was from ACME (ACME S.r.l., Cavriago, Italy). Trypsin from bovine pancreas, bovine serum albumin (BSA), glucono-δ-lactone (GDL), DL-dithiothreitol (DTT), iodoacetamide (IAA), ammonium bicarbonate (ABC), formic acid (FA), and acetonitrile (ACN) were purchased from Merck (Merck KGaA, Darmstadt, Germany). Dulbecco's modified eagle's medium (DMEM), L-glutamine, streptomycin, penicillin, Na-pyruvate, and the non-essential amino acids (NEAA) were obtained from Gibco (Thermo Fisher Scientific, Waltham, MA, USA). Fetal serum bovine (FBS) and Dulbecco's phosphate buffered saline (DPBS) were from Euroclone (Milan, Italy). Protein assay dye reagent concentrate was from Bio-Rad. Resazurin sodium salt was from Alfa Aesar (Ward Hill, MA, USA). All solvents were of reagent grade with the highest purity available. Deionized ultra-filtered water was used throughout this study.

2.1.2. Bacterial lysates preparation and quantification

Two L. *bulgaricus* (LB) strains, 1865 and 1932, belonging to the microbial culture collection of the University of Parma (UPCC), were maintained as stock cultures at −80 °C in MRS broth (Oxoid, Basingstoke, UK) supplemented with 20 % (v/v) glycerol until use. LB 1932 was chosen as a well-known EPS producer. Bacteria were recovered in MRS broth by two sub-culturing steps (2 % v/v) at 42 °C under anaerobiosis obtained with AnaeroGen gas packs (ThermoFisher Scientific Italia, Rodano, MI, Italy). Before use, the cultures were harvested by centrifugation (10,000 g, 10 min at 4 °C), saving supernatants for further analysis. The collected bacteria were washed twice in sterilized water to remove any media residues and resuspended to the original density. The bacterial lysates were obtained using a sonicator (Sonoplus HD3100, Bandelin, Berlin, Germany) by performing 5 cycles of treatment consisting of 1 min of sonication at the power of 53 W then 1 min of pause. While treated, bacteria suspensions were kept in an ice bath to avoid any overheating. The obtained bacterial lysates were named respectively L18 and L19. From each lysate, LB derivatives, i.e., soluble fractions, cell-bound EPS, released EPS and proteins, were collected (Table 1).

2.1.3. Preparation and quantification of lysates soluble fraction

Raw lysates L18 and L19 were used to prepare the corresponding soluble fraction (SF). Samples were centrifugated at 6000 g for 20 min and the supernatants were filtered using a 0.22 μm pore filter (Sartorius, Germany) to remove any whole bacteria remaining. SF18 and SF19 were

Table 1
L. *bulgaricus* derivatives used in this study and their abbreviations.

L. *bulgaricus*	LB1865	LB1932
Raw lysate	L18	L19
Soluble Fraction	SF18	SF19
Cell-bound EPS	c-EPS18	c-EPS19
Released-EPS	r-EPS18	r-EPS19
Proteins extracted from Soluble Fraction's Pellet	P18	P19

thus obtained and the remained pellets, after being solubilized, were assayed for protein content using the procedure described below.

2.2. LB proteins

2.2.1. Protein extraction, quantification, and preparation for LC-MS/MS analysis

Total proteins were extracted from 1 mL of each raw lysate (L18 and L19), the soluble fraction (SF18 and SF19) and the pellet (P18 and P19) by adding 8 M urea. Samples were vortexed and put on a stirring plate at 500 g for 15 min, then sonicated for 30 min at 4 °C. Extracts were centrifuged at 4 °C for 10 min at 10000 g and the supernatants were concentrated with a buffer exchange procedure using 50 mM ammonium bicarbonate (Amicon® Ultra 0.5 mL centrifugal filters; 3-kDa MW cut-off). Protein extracts were assayed for total protein content according to the Bradford procedure.

Proteins were reduced and alkylated with DTT (100 mM for 30 min at 37 °C), followed by IAA (200 mM for 30 min in the dark), and the addition of DTT (100 mM for 15 min at room temperature). Finally, samples were digested by incubation with trypsin (1:50 enzyme/substrate ratio) at 37 °C overnight, then stopping the digestion with 1 μL of FA. All samples were dried under nitrogen flow and reconstituted with 50 μL of a water/acetonitrile/formic acid aqueous solution (49.95/49.95/0.1, v/v) for qualitative mass spectrometry analysis. Each sample was extracted in duplicate ($n = 2$ biological replicates).

2.2.2. LC-LTQ-Orbitrap XL analysis

Peptide separation of the tryptic digests was carried out by using an Xbridge Peptide BEH C18 (250 × 2.1 mm, 5 μm) column (Waters, Milford, MA, USA) equipped with a pre-filtering column. Eluting mixtures included solvent A (0.1 % aqueous formic acid, v/v) and B (0.05 % formic acid in acetonitrile, v/v) delivered under gradient elution at the flow rate of 200 μL/min. The gradient was set as follows: 0 min 2 % solvent B, 4 min 2 % solvent B, 150 min 90 % solvent B, 155 min 90 % solvent B, 170 min 2 % solvent B. The mobile phase was delivered by a Dionex Ultimate 3000 liquid chromatographic (LC) system (Dionex Corporation, San José, CA, USA) equipped with a 100-vial capacity sample tray. The volume of the injected samples was 5 μL. Qualitative protein analysis was obtained by mass spectrometry using an LTQ linear ion trap-Orbitrap XL instrument (ThermoScientific Corporation, San José, CA, USA), equipped with an electrospray source (ESI) interface and controlled by Xcalibur software. Optimized conditions of the interface were: capillary voltage 3 kV, capillary voltage 13 V, capillary temperature 275 °C, tube lens 100 V, sheath gas flow, auxiliary gas flow, and sweep gas flow delivered at 40, 10, and 5 arbitrary units, respectively. In the first scan event (full scan), the m/z window was 250–2000 with a resolution of 3000. The four highest m/z ratios over the threshold of 1000 counts were selected for collision-induced dissociation (CID) in the ion trap, with a normalized collision energy of 35 % in the collision cell. Each sample was analyzed twice ($n = 2$ instrumental replicates).

2.3. LB lipids

2.3.1. Extraction and preparation for mass spectrometry analysis

Total lipids were extracted from 1 mL of each raw lysate (L18 and L19) re-adapting the procedure proposed by Bligh & Dyer [40]. A mixture of chloroform: methanol (2:1 v/v) was added to each lysate in a 1: 1 ratio (v/v), the mix was vortexed, centrifuged at 5000 g for 5 min and the organic phase was collected; the procedure was repeated twice. The organic phases were combined, dried under a nitrogen flow, and reconstituted with 200 μL of hexane for target mass spectrometry analysis. Each lysate was extracted in duplicate ($n = 2$ biological replicates).

2.3.2. LC-MS/MS SRM analysis

Lipid target analysis was carried out by liquid chromatography with tandem mass spectrometry in selective reaction monitoring mode (LC-MS/MS SRM). Each solution was eluted by using an Atlantis dC18 column (150 × 2.1 mm, 5 μm; Waters, Milford, MA, USA) equipped with a C18 pre-filtering column. An elution system based on a solvent gradient (solution A: acetonitrile; solution B: methanol) was delivered at 0.2 mL/min. The gradient was set as follows: 0 min 50 % solvent B, 5 min 80 % solvent B, 8 min 95 % solvent B, 17 min 50 % solvent B until 25 min. The mobile phase was delivered by the Agilent HP 1200 chromatographic system (Agilent Technologies, CA, USA) equipped with a 100-vial capacity sample tray (injection volume: 10 μL; $n = 2$). A QTRAP 4000 triple quadrupole mass spectrometer (ABSCIEX, Foster City, USA), equipped with a pneumatically assisted ESI interface was used. The sheath gas (nitrogen, 99.999 % purity) and the auxiliary gas (nitrogen, 99.998 % purity) were delivered at flow rates of 45 and 5 arbitrary units, respectively. Source parameters were as follows: ESI voltage 5.5 kV, capillary voltage 50 V, capillary temperature 350 °C. Experiments were performed under positive and negative ion-SRM conditions using nitrogen as collision gas (pressure of 2.1×10^{-3} mbar) and a 50 ms-dual time for each transition monitored. The SRM transitions monitored were reported in Table S1 and S2 (Supplementary Materials). Each sample was analyzed twice ($n = 2$ instrumental replicates). The analytes were relatively quantified among samples by normalization with total protein content.

2.4. LB exopolysaccharides

2.4.1. Extraction

EPS were extracted from both L. *bulgaricus* strains and the relative culture medium re-adapting the procedure proposed by Kun Wang et al. [41]. Cell-bound EPS (c-ESP) were extracted from the raw lysates (c-EPS18 and c-EPS19), while the released EPS (r-EPS) were extracted from the supernatants (r-EPS18 and rEPS19). EPS were precipitated in ethanol (1:3 v/v ratio) overnight at 4 °C after gently mixing. The solution was centrifuged at 5000 g for 45 min, the supernatant was eliminated and the pellet was dispersed again in a volume of ultrapure water equal to the initial volume of the sample. This procedure was repeated twice. To remove proteins, acetone precipitation was carried out by incubating the samples overnight at 4 °C and then centrifuging at 9000 g for 2 min. The supernatant, containing EPS, was collected and dried under nitrogen flow.

2.4.2. ATR FT-IR spectroscopy

FTIR spectra were performed in the attenuated total reflection mode (ATR), using a Perkin-Elmer spectrometer (Norwalk, CT, USA). The apparatus works with a single reflection at an incident angle of 45°. The analysis was carried out on r-EPS and c-EPS from both L. *bulgaricus* strains at room temperature and ambient humidity. For each spectrum, 32 scans were acquired between 4000 and 400 cm^{-1} with a spectral resolution of 2 cm^{-1}.

2.5. ALG/HA self-crosslinking inks for 3D printing

2.5.1. Ink preparation for 3D printing

Sodium alginate (6 % w/v), hyaluronic acid (10–20–30-40 % of ALG weight) and calcium carbonate (160 mM) powders were dispersed in ultrapure water in a beaker and magnetically stirred for 48 h until a homogeneous dispersion was achieved. 1 mL of the ALG/HA/CaCO$_3$ dispersion was first sonicated in an ultrasonic bath (Branson 2510; OPTO-LAB, Modena, Italy) for 30 min at room temperature and then carefully and quickly mixed with 1 mL of a freshly prepared GDL water solution as previously reported [33]. Different GDL concentrations (80, 100, 120 and 140 mM; pH = 4.5 ± 1) were tested. For hydrogels containing L. *bulgaricus* derivatives, the final inks were prepared by using GDL solubilized in the LB derivative solutions.

2.5.2. 3D printing and hydrogel production

A custom-built low-temperature manufacturing system was designed and developed by combining a Peltier cell with a homemade Fuse Deposition Manufacturing (FDM) 3D printer, as previously described [33,42]. The ink formulation based on ALG, HA, $CaCO_3$ and GDL was loaded into a 5 mL syringe and extruded through a 26 G needle (inner diameter 0.260 mm) by application of controlled pressure to the syringe through a mechanically assisted piston (see Table S3 and Table S4 for ink composition). The deposition took place through a robotic arm that moves along three axes (x, y, z) following the directives imposed by the g.code file on a stainless-steel cold Peltier cell ($-14\ °C$). For each ink formulation, a square hydrogel (grid 1.6 cm × 1.6 cm in size of parallel overlapped filaments with a distance of 200 μm) was printed similarly as previously reported [33]. Once terminated the deposition, the hydrogel was post-printing processed at $-2\ °C$ to complete the self-gelation process (from 4 up to 7 days, as a function of the number of layers and composition). After the gelation time, the hydrogels were brought to RT to allow the detachment from the steel plate and stored at 4 °C until use.

2.5.3. Scanning electron microscopy (SEM) analysis

SEM morphological characterization was conducted on the 3D printed alginate-based hydrogels. The hydrogels were dehydrated by immersion twice for 10 min in increasing grades of ethanol from 50° to absolute. Anhydrous hydrogels were obtained by the critical point drying technique (Balserz Union, Lake Butler, FL, USA) to avoid structure deformations. The anhydrous hydrogels were then fixed on support using double-sided carbon tape, sputter coated with gold (thickness 60 nm) (E5100, Polaron, Quorum Technologies Ltd., Leves, UK) and observed by SEM (Philips 501, Philips, Eindhoven, The Netherlands).

2.6. In vitro-fibroblast cell culture studies

Primary human skin fibroblasts, coded as C86, were derived from a forearm biopsy of a healthy donor after the signature of an informed consent. Cells were maintained in a standard culture medium: formed by DMEM supplemented with 1 % (v/v) of L-Glutamine, 1 % of Streptomycin and penicillin, 1 % of Na-pyruvate, 1 % NEAA and 10 % FBS. All the LB derivatives were dried under nitrogen flow, sterilized under a UV lamp for 2 h and reconstituted in the assay medium. Table 2 summarized the in vitro experiments performed on fibroblast cells.

2.6.1. Cytotoxicity test of L. bulgaricus derivatives

The cytotoxicity of LB derivatives was tested on C86 fibroblast cells seeded in a 96-well plate at 4000 cells/well (150 μL standard medium). After 24 h of incubation at 37 °C and 5 % CO_2, the standard medium was removed and replaced with a medium enriched with LB derivatives. Their cytotoxicity was assessed after 24 h and 72 h using the resazurin assay. The treatment concentrations evaluated in the various tests are summarized in Table 2. Six replicates were performed for each of the six conditions and the control (Ctrl). At each time point, the cell media enriched with LB derivatives were aspirated, the cells were gently washed in PBS to remove eventual debris and 110 μL resazurin solution (10 μg/mL) was added to each well. Plates were incubated for 2 h at dark at 37 °C in a wet atmosphere with 5 % CO_2 and 95 % humidity. Fluorescence was recorded at 540 nm excitation and 590 nm emission by a Spark® 10 M microplate reader (Tecan, Switzerland). The fluorescence values of the control wells were considered as 100 % of viability.

2.6.2. In vitro wound healing model

A scratch test was performed to evaluate the migration of fibroblast cells treated with LB derivatives, as an in vitro wound healing model. Fibroblast cells were cultured in a 48 well-plate (20,000 cells/well, 400 μL standard medium) for 48 h in standard conditions to reach ~90 % confluence. After this time, the standard medium was removed, and the cell monolayers were scratched using a 200 μL sterile pipet tip to create a uniform cell-free gap area with reproducible width of wounding. Debris

Table 2
Scheme of the in vitro tests, time points, LB derivatives and concentrations evaluated on fibroblast cells.

Test	Time (h)	SF[a] (μg/mL)	r-EPS[b] (μg/mL)	P[c] (μg/mL)
Cytotoxicity test 1 (LB derivatives dissolved in medium; resazurin assay)	24/72	50	2000	50
Cytotoxicity test 2 (LB derivatives dissolved in medium; resazurin assay)	24/72	25	20	25
Scratch test 1 (In vitro wound healing model)	0/8/24/48	25	20	25
Scratch test 2 (In vitro wound healing model)	0/8/24/48	50	40	50
Proliferation test on hydrogel-loaded treatments (resazurin assay)	24/72	3.4 μg/well	3 μg/well	[d]
Proliferation test for protein biomarkers evaluation by target mass spectrometry analysis	48	25	20	25
Viability test in parallel to mass spectrometry analysis. (Treatments dissolved in medium; resazurin assay)	48	25	20	25

[a] Soluble Fraction of raw lysates of LB1865 and LB1932 strains.
[b] r-EPS from LB1865 and LB1932 strains.
[c] Protein extracted from the pellet of raw lysates of LB1865 and LB1932 strains.
[d] Not tested.

was removed from the culture by gently washing each well with sterile PBS. The cells were then incubated with the medium enriched with the LB derivatives (SF18 and 19; r-EPS 18 and 19; P18 and 19, according to the scheme reported in Table 2), at 37 °C in a 5 % CO_2, 95 % humidity atmosphere. Four replicates were made for each treatment condition, the positive control (standard medium with 10 % FBS; $Ctrl^+$) and the negative control (standard medium with 2 % FBS; $Ctrl^-$) (n = 4). Two independent scratch tests were performed. Cell migration was monitored by microscopy using an inverted light microscope (Leica DMi1, Leica Microsystems, Milan, Italy) and images were captured (45× magnification) at different time points (0, 8, 24, 48 h) after the injury.

At each time point, the gap was photographed at two different points for each well. To calculate the % wound closure, the images collected were analyzed quantitatively using the public domain ImageJ software v. 1.53e (NIH, Bethesda, MD, USA). The quantification of relative wound closure was evaluated according to the following equation:

$$Wound\ clousure\ (\%) = \frac{A_0 - A_t}{A_0} \times 100$$

where A_t is the wound area at time t and A_0 is its initial area.

2.6.3. Cell proliferation test on 3D hydrogels functionalized with L. bulgaricus derivatives

The resazurin assay was performed to estimate cell proliferation on 3D-printed hydrogels containing SF19 and r-EPS19. After the first 24 h of cell culture in a standard medium supplemented with 10 % FBS, the latter was replaced by a standard medium with 2 % FBS, in which the functionalized hydrogels were inserted to the bottom of the wall. Before use, the 3D hydrogels were brought to dryness, punched (6 mm diameter) and sterilized under a UV lamp for 2 h. LB derivative quantities present in each hydrogel piece are indicated in Table 2. Each treatment was tested in quadruplicate (n = 4).

2.6.4. Study of cell mechanisms through protein biomarkers

Fibroblast cells were seeded in 6-well plates (170,000 cells/well, 2 mL standard medium) for proteomic analysis and in 96-well plates (5000 cells/well, 150 μL standard medium) to assess cell viability

(incubation time 24 h, 37 °C, 5 % CO_2, 95 % humidity). Then, the medium was replaced by a serum-free one, enriched with LB derivatives (SF18 and 19; r-EPS 18 and 19; P18 and 19, Table 2, $n = 6$) for 48 h.

For proteomic analysis, adherent cells were washed with PBS, detached using trypsin solution (250 μL/well) and collected in a small tube after centrifugation. Cell pellets were further washed with fresh PBS 3 times and stored at −20 °C until protein extraction. Total proteins were extracted and quantified, and samples were prepared for LC-MS/MS analysis following the protocol described in paragraph 2.2.1.

The tryptic peptides were reconstituted in 100 μL of 0.1 % (v/v) formic acid aqueous solution and 50 % (v/v) acetonitrile before LC-MS/MS to identify and monitor the distribution of protein regeneration biomarkers using the SRM approach. Samples were analyzed as biological ($n = 2$) and technical replicates (n = 2) using the same LC separation reported in the previous section (paragraph 2.3.2). As for semiquantitative analysis, experiments were performed under positive ion-SRM conditions using nitrogen as collision gas (pressure of 2.1×10^{-3} mbar in the collision cell; declustering potential 80 V, collision energy 40 V) and a 20 ms-dual time for each transition monitored. The SRM transitions monitored were reported in Table S5.

2.7. Data evaluation

2.7.1. Bioinformatic analysis and mass spectrometry data processing

LC-LTQ-Orbitrap XL raw data were processed using the Proteome Discoverer software (v. 1.6, Thermo Fisher Scientific) with SEQUEST as the search algorithm. Raw files were processed using precursor ion tolerance at 0.1 amu and fragment tolerance at 0.5 amu. Processed files were then searched against the L. *bulgaricus* database to obtain the total number of proteins identified in samples. LC-LTQ-Orbitrap XL raw data were processed also using MaxQuant software (v. 1.6.2.10) in label-free mode using FASTA sequences of L. *bulgaricus* ATCC 11842 (taxid: 390333) proteome downloaded from Uniprot. The software was set up to recognize the specific digestion of trypsin, allowing for a maximum of 2 missing cuts, setting N-terminal acetylation and methionine oxidation as variable modifications and the carbamylation of cysteines as a fixed modification. Then, data were reprocessed by Perseus software (v.1.6.15.0) to qualitatively compare the proteins extracted from the two different strains. Only identified by site, reverse and potential contaminants filters were applied, to exclude proteins not correctly identified and potential contaminants.

A panel of 14 proteins involved in tissue regeneration were considered for the target mass spectrometry assay. FASTA protein sequences were obtained from Uniprot Human proteome database and SRM transitions for each protein were simulated by Skyline (v. 20.0, SCIEX, Redwood City, CA, USA), setting trypsin as digestion mode with no missed cleavage and carbamidomethylation of cysteines as structural modification (Table S5). The uniqueness of candidate peptide sequences was assessed by BLASTp tool (basic local alignment search tool; www.ncbi.nml.nih.gov link NCBI BLAST) search (algorithm: blastp; ATRIX PA 30; GAP COASTS: existence 10, extension 1; DATABASE: non-redundant protein sequences) from NCBI (National Center for Biotechnology Information) (Bethesda, MA, USA). All LC-MS/MS SRM data (target proteins and lipids analysis) were analyzed using the Analyst v 1.4 software, and integrations of the peaks' areas were obtained by the MultiQuant program (version 2.1, ABSCIEX). For the protein biomarkers study, Perseus software was used to cluster the samples: for all data relating to the abundance of each protein considered in each sample, the Z-score was calculated. For each measure group relating to a single protein abundance in the various samples, the mean and the standard deviation were calculated, then the mean was subtracted from each value of the group, and the result was divided by the standard deviation. Data thus transformed were used for the construction of a heatmap through clustering based on the calculation of Euclidean distances.

2.7.2. Statistical analysis

Statistical analyses were performed applying the t-Student test at the 95 % significant level using the Microsoft Excel software. All experiments were performed at least in triplicate and the results were expressed as the mean ± standard deviation (SD).

3. Results and discussion

3.1. Characterization of L. bulgaricus derivatives

To increase the understanding of the potential therapeutic efficacy of some LB derivatives in wound healing, the first part of the study was focused on the isolation of the main classes of chemical compounds (i.e., proteins, lipids, and EPS) expressed by both LB stains (LB1865 and LB1932) and the qualitative/quantitative characterization of these extracts. The knowledge of the exact composition of bioactive components in these extracts is pivotally related to their applications in regenerative medicine, as the activity of such complex extracts on cell behavior is strictly connected to their chemical composition and can be related to a predominant defined class of compounds or be synergistic. It is also essential for further development steps, such as standardization and certification of quality processes.

3.1.1. Quali- and quantitative analysis of LB proteins

Proteins in the raw lysate L18 and L19 were considered at first. The percentage of the total protein content, quantified both in the soluble fraction and in the pellet of the raw lysate, exhibited highly significant quantitative differences between the two strains. SF18 contained 50 % w/v of proteins and its corresponding pellet (P18) the 30 % w/w. Only 5 % w/v of proteins was present in SF19 while most of the proteins precipitated in the pellet (P19: 88 % w/w). This difference could be largely explained by considering that compared to LB1865, LB1932 is a well-known producer of cell-bound EPS that could link proteins and/or lipids (as biofilm) to lysate fragments and increase their precipitation during the centrifugation step. Furthermore, these differences could also be related to a different structure of the EPS (linear or branched) or composition, which could lead to different functions and binding abilities [43].

Proteins extracted from both lysates were thus characterized by liquid chromatography-high resolution mass spectrometry. Among the almost 4000 identified proteins, only 22 % of them were common to the two strains (Fig. S1 A-B). Mainly, these common proteins were identified as those involved in basic metabolic and energy processes, or ribosomal and chaperonin proteins (Fig. S1 C).

3.1.2. Lipid characterization by LC-MS/MS SRM analysis

Lipids extracted from raw lysates were characterized by LC-MS/MS SRM analysis, grouped into lipid classes and their relative abundances measured and compared between strains (Table S6). Among the free fatty acids, palmitic acid (C16:0) and oleic acid (C18: 1), were the most abundant ones. For both strains, it was possible to identify, in low amount and without differences in relative abundance, the C19:0 cyc fatty acid, a characteristic compound of the lactobacilli membrane with a saturated hydrocarbon chain with 19 carbon atoms bringing a cyclopropane ring. This molecule has an important role in maintaining membrane fluidity, and its production increases under stress conditions such as variations in osmolarity, the presence of ethanol and acidity [44]. Triacylglycerols (TAG) data were comparable between the two strains. Similar results were obtained for the lysyl-phosphatidylglycerides (LPG) data, considered characteristic of the membranes of Gram-positive bacteria [45], with the exception of LPG 17:1, LPG 16: 1 and LPG 20: 4 which were detected only in LB1865. Finally, as for the phosphatidylglycerides (PG) class, the PGs 14: 0–18: 2, 16: 0–18: 0 and 16: 0–18: 1 had been identified exclusively in LB1865, while the PGs 14: 0–18: 1 and 16: 0–18: 2 were detected in higher amounts in LB1932.

3.1.3. EPS characterization by ATR FT-IR spectroscopy

The last characterization step involved the extraction and characterization of the extracellular microbial exopolysaccharides. Cell bound and released EPS (c-EPS and r-EPS) were examined. Generally, LB1932 strain was able to express r-EPS up to 90 % more than the LB1865 strain.

The ATR FT-IR spectrum of r-EPS from LB18 or LB19 were then acquired and compared (Fig. S2). Spectra did not show significant differences between r-EPS18 and r-EPS19. In both spectra there is the stretching of the O—H bond (r-EPS18: 3284 cm^{-1}; r-EPS19: 3271 cm^{-1}), that of the C—H bond (r-EPS18: 2929 cm^{-1}; r-EPS19: 290026 cm^{-1}); peak at 1637 cm^{-1} is indicative of protein presence and is associated with the NH bond bending, the peaks at 1453 cm^{-1} (r-EPS18) 1457 cm^{-1} (r-EPS19) indicate the symmetrical stretching of the COO- group, while the peaks at 1242 cm^{-1} and at 1216 cm^{-1} for r-EPS18 and for r-EPS19 respectively, suggest the possible presence of sulfated groups [46]. Finally, some peaks related to glycosidic bonds (r-EPS18: 1043 cm^{-1}; r-EPS19: 1019 cm^{-1}), confirm the presence of carbohydrates [17]. The same profile was obtained for c-EPS18 and c-EPS19 (spectra not shown).

3.2. Optimization of the self-crosslinking formulation for 3D printing

The second part of this work was focused on the development of ALG and ALG/HA-based self-crosslinking bioinks to support the 3D printing manufacturing of hydrogels incorporated with hydrophilic bioactive substances. These bioinks should allow the 3D printing process via room-temperature extrusion from a mechanically driven syringe and be able to retain the hydrogel 3D structure when extruded on a −10 °C stainless steel plate. The cross-linking mechanism should then occur after printing to prepare hydrogel with a well-defined 3D structure and mechanical properties suitable for use as wound dressing [33].

A formulation previously developed by our research group (3 % ALG (w/v), 80 mM CaCO$_3$ and 140 mM GDL) [33], was used as a starting point and optimized as a function of different combinations of ALG/CaCO$_3$/GDL and content of LB derivatives (raw lysate or soluble fraction). Parameters, such as the pH of the bioinks, the number of printable layers, the maximum ink extrusion time, the curing time at 2 °C necessary to complete the hydrogel self-crosslinking, and the capacity of the 3D printed hydrogel to retain its structure in water were evaluated (Table S3). The monitoring of these parameters was crucial to print structured hydrogels with proper mechanical characteristics. The internal gelation process is pH dependent, as the acidification of the alginate-based suspension containing calcium carbonate, due to the GDL hydrolysis, drives the release of Ca^{2+} which become available for the formation of the "egg-box" structure [47]. An increase in the concentration of GDL in solution leads to a faster cross-linking reaction, reducing both the ink homogeneity and maximum extrusion time, due to the increased viscosity. A summary of the different combinations tested to prepare 3D-printed functionalized hydrogels containing LB derivatives is reported in Table S3. In general, the addition of raw lysates or their soluble fractions to ALG-based formulations seemed to have an accelerating effect on the ink cross-linking kinetics, reducing the printability of the solution which can be attenuated by reducing the concentrations of GDL.

Several combinations can allow 3D manufacturing of functionalized hydrogels, but the best results in terms of number of printable layers and stability were obtained with the following combination: 3 % ALG (w/v), 80 mM CaCO$_3$, 80 mM GDL aqueous solution (final volume 0.5 mL) and 0.5 mL of LB sample extract (final volume of the ink: 1 mL). To confirm the quality of the 3D constructs, ALG hydrogels were characterized morphologically by SEM (Fig. S2) to evaluate the 3D macrostructure. The ALG hydrogel presented a well-defined 3D macrostructure with homogeneous surface and filament inner pore distribution (pore size distribution between 3 and 52 μm) (Fig. S3 A-C).

Here HA, extensively used in wound healing and regenerative medicine [48–50] was added to the optimized ALG ink formulation, to further improve the properties of the 3D printed hydrogel. One of the main characteristics of HA is the capacity to attract water molecules, therefore, in combination with ALG, it increases the hydrophilic character of the resulting hydrogels, promoting cell adhesion [48]. ALG/HA ink formulations were prepared by keeping constant the final concentrations of ALG (3 % w/v) and CaCO$_3$ (80 mM) but testing different concentrations of HA and GDL as summarized in Table S4. During the preparation of ALG/CaCO$_3$/HA suspensions, an increase in the viscosity of the formulation proportional to the increase in the quantity of HA was observed. An increase in viscosity was already reported to hinder the molecular movement of ALG chains increasing the time required for gel formation [31]. In our case, this resulted into an increase in the extrudability time of the solution and in a rise of the curing times of the ink. The preliminary tests reported in Table S4 allowed us to select the ink formulation based on ALG (3 % w/v), HA (40 % w/w), GDL (80 mM) for further test with the LB derivatives. 80 mM GDL was the best compromise for inks containing raw lysates, whereas 140 mM GDL allowed for the use of the LB soluble fractions (SF). The use of EPS was carefully tested and excellent printability was obtained under the same conditions used for the soluble fraction. The SEM analysis of ALG/HA hydrogels allowed to evidence that HA did not interfere with the quality of the final morphological structure, both in terms of macrostructure and homogeneous surface and filament inner pore distribution (pore size distribution between 5 and 48 μm) (data not shown).

All these data showed that the production of a variety of self cross-linking ink formulations possibly used for manufacturing hydrogels with the minimum requirements described above is allowed, supporting the new critical need to develop advanced inks. Finally HA has been studied for its antimicrobial properties for the progress of the next generation antimicrobial therapeutic strategies for the control of infections associated with health care [51], for example HA films were effective as antimicrobial towards a common pathogen *Staphylococcus aureus* at the same time allowing a good proliferation of human fibroblasts [50]. These insights suggest hints for a possible antimicrobial activity of the 3D printed hydrogels here developed; which could be promising to investigate against Gram + and Gram - pathogens (e.g. *Pseudomonas aeruginosa* and *Staphylococcus aureus*) to support future applications in the biomedical field.

3.3. Effect of lysates' derivatives on in vitro-fibroblast cell cultures

3.3.1. Cytotoxicity test of L. bulgaricus derivatives

The biocompatibility of LB derivatives was evaluated over fibroblast cells and the results were summarized respectively in Fig. 1. In this first test, a dramatic cytotoxic effect was recorded for r-EPS within 24 h for both LB strains at the concentration tested (2000 μg/mL).

The properties of EPS strictly depend on several factors (i.e. structure, size, branching, composition, positive and negative charges, viscosity, purity, etc.) [52,53]. In our studies, ATR-FT-IR experiments suggested the presence, in the EPS extracts, of sulfate groups and proteins. The EPS-fibroblast physico-chemical interaction behavior is difficult to elucidate, but this partially purified extract strongly affected different cell communication mechanisms including apoptosis. A dose-dependent activity was demonstrated as no signs of toxicity were observed by lowering r-EPS concentration at 20 μg/mL. The soluble fraction of the two LB strains tested at the same protein concentration level (50 μg/mL) showed a different opposite behavior. In particular, SF18 improved ($p > 0.05$) cell proliferation, whereas the SF19 decreased cell activity up to 60 % in 72 h. Finally, at 72 h, treatments with the protein extracted from the pellets (P18 and P19), after an initial reduction in cell proliferation, allowed for significant cell growth. In a second test, with lower concentrations of the same treatments [SF (25 μg/mL); P (5 μg/mL)], no significant cytotoxic effects were shown.
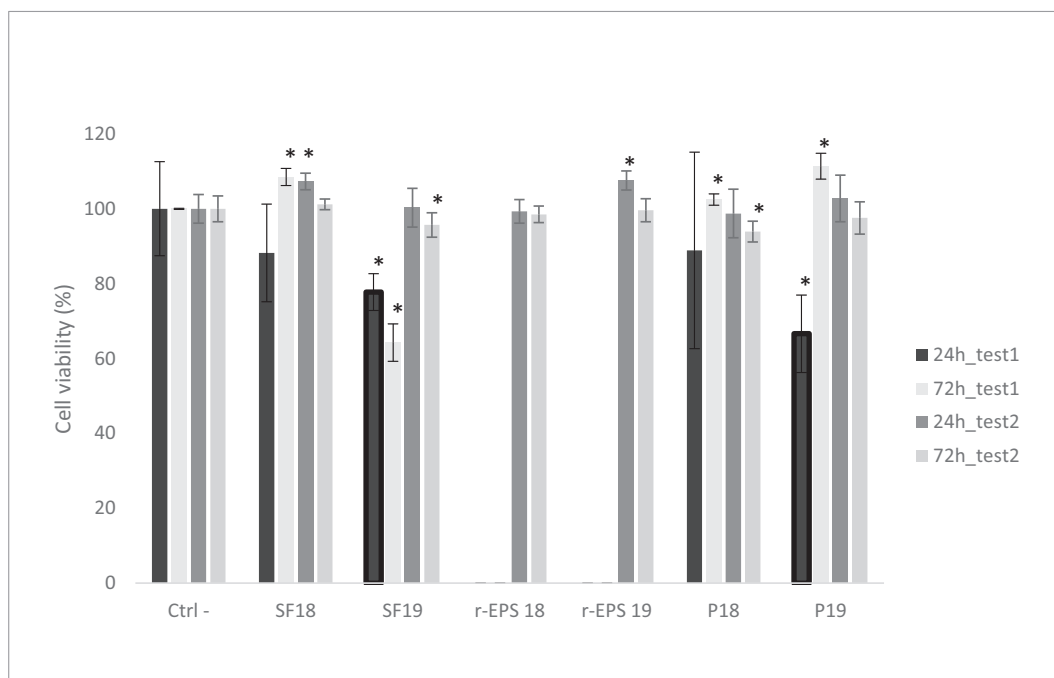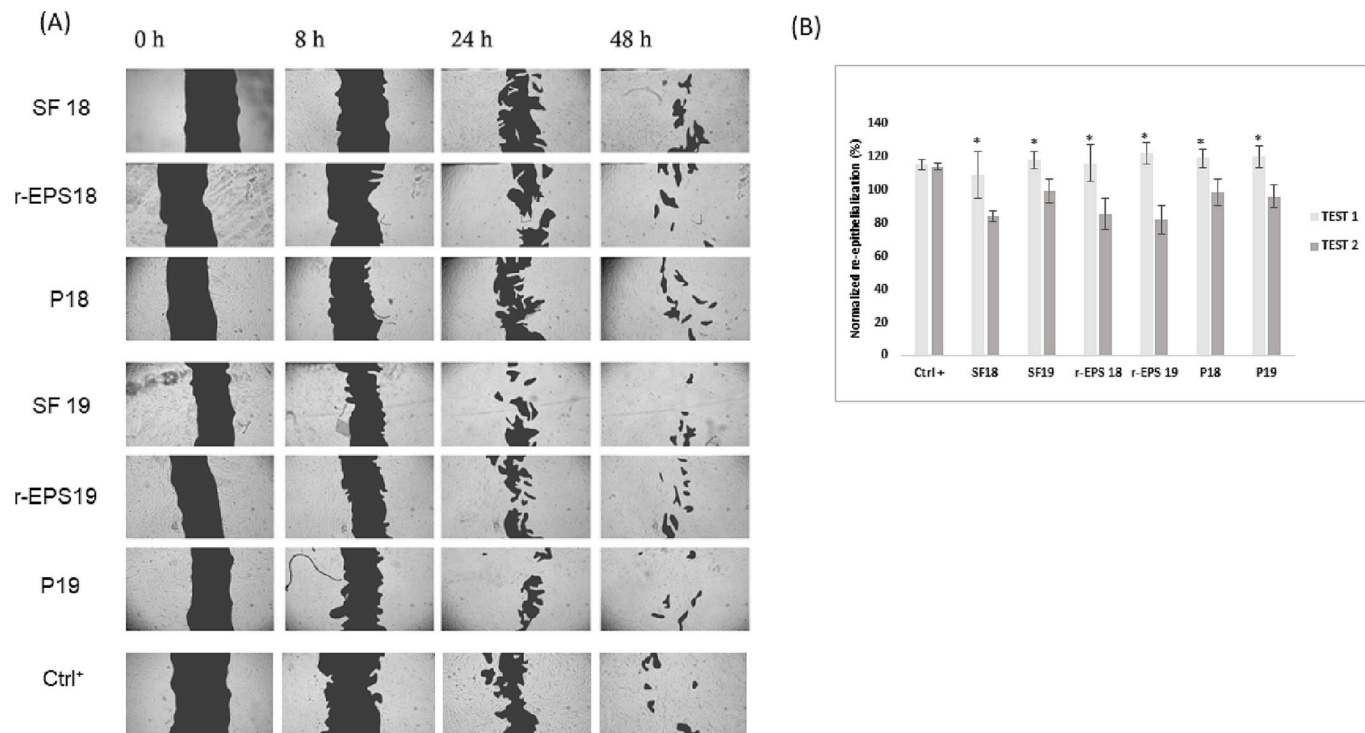
Fig. 1. Effect of L. *bulgaricus* derivatives on fibroblast cells viability at 24 h and 72 h. Cytotoxicity Test 1 treatments: SF (50 μg/mL), r-EPS (2000 μg/mL), P (50 μg/mL). Cytotoxicity Test 2 treatments: SF (25 μg/mL), r-EPS (20 μg/mL), P (25 μg/mL). Results are reported as mean ± standard deviation of six independent measurements. The results are expressed as a percentage of viability compared with the negative control (Ctrl-) for samples treated with various L. *bulgaricus* derivatives; statistically significant differences ($p < 0.05$, T-student test) between the samples and the relative control are indicated with asterisk (*).

3.3.2. Evaluation of fibroblast migration treated with L. bulgaricus derivatives

The ability of LB derivatives to stimulate the migration of fibroblasts, showing thus a regenerative potential, was evaluated by scratch test. To this aim an artificial discontinuity was created on the cell monolayer at confluence, a fundamental condition to avoid confounding overlap

Fig. 2. Effect of *L. bulgaricus* derivatives on fibroblast cells migration from 0 to 48 h. (A) Images from the first scratch test for the various treatments, and the positive control, over time (from 0 to 48 h). The photographs, taken under a microscope, were used to calculate the scratch area (highlighted in black) using the ImageJ software. (B) Comparison between scratch test 1 and scratch test 2 at 48 h. Results are reported as mean ± standard deviation of four independent measurements. The results are reported as the mean percentage of normalized re-epithelialization on the respective negative control; statistically significant differences (p < 0.05, T-student test) between tests 1 and 2 are indicated with asterisk (*).

between the effects of cell proliferation and migration [54,55]. As previously reported in Table 2, two scratch tests were performed. The first test (Test 1) highlighted that the scratch area decreases over time (from 0 to 48 h) until they become almost non-detectable at 48 h, with improved migration effects for the derivatives of the LB1932 strain (Fig. 2A). A further scratch test (Test 2) was performed by doubling LB derivative concentrations, and the results were compared by normalizing the re-epithelialization data obtained for the two tests on the respective negative control (Ctrl-). Fig. 2B shows the comparison at 48 h, the last and significant time point. Scratch test 1 gave the best re-epithelialization rates in all samples ($p < 0.05$, T-student test) allowing us to conclude that the best effects, for stimulating cell migration, were those obtained under the conditions of Test 1.

3.3.3. Cell proliferation test on 3D hydrogels functionalized with L. bulgaricus derivatives

Based on the collected results, cell proliferation tests on functionalized hydrogels were carried out by selecting the soluble fraction and the r-EPS derivatives deriving from the LB1932 strain, as they provided the best performance. The use of proteins extracted from the pellet was excluded because the related cultures showed the presence of aggregates in the medium upon microscopic observation (data not shown).

Treatments selected above were used to produce self-crosslinking 3D hydrogels as described in paragraph 2.6.3. To evaluate cell proliferation, viability measurements were performed, using resazurin assay, at 24 and 72 h on fibroblast cells grown in the presence of hydrogels.

In a first step, cell viability data obtained for the samples grown on nude wells (Ctrl) were compared with those grown in the presence of the unloaded hydrogel (Ctrl Hydrogels); a statistically significant reduction of cell viability for Ctrl Hydrogels, at 24 and 72 h ($p < 0.05$, t-student test), was detected compared to those grown on the nude wells. However, Ctrl Hydrogels allow cell viability of 84–86 % at 24 h and 72 h respectively if compared to the Ctrl samples. According to guidelines for the evaluation of in vitro cytotoxicity for medical devices and delivery systems (ISO 10993-5: 2009), these data confirmed the biocompatibility of Ctrl Hydrogels that showed vitality values above the 70 % threshold [56].

In a second step, functionalized hydrogels were considered (Fig. 3). Fibroblasts incubated in the presence of functionalized hydrogels showed an increase in cell viability compared to the Ctrl Hydrogels indicating an increase in their proliferation. This increase was higher at 24 h and comparable at 72 h for both treatments. In detail, it is more pronounced in the SF19 hydrogels samples, where it settled around 20

%, compared to the r-EPS19 hydrogels samples, where it settled around 10 %.

In conclusion, in these experimental conditions, the hydrogels functionalized with the soluble fraction or with r-EPS of LB1932 strain have a positive effect on fibroblasts growth.

### 3.3.4. Regeneration protein biomarkers study

In an endeavor to further investigate the effect of L. *bulgaricus* derivatives on fibroblast cells, a set of protein biomarkers involved in extracellular matrix modelling, proliferation, wound healing, and apoptosis processes were analyzed by LC-MS/MS SRM target analysis. Initially, in parallel to the cell cultures intended for proteomic analysis, a viability test with resazurin assay was performed as a control on the culture conditions used, confirming, as expected, the non-cytotoxicity of the treatments, at the concentrations used (Table 2), also in combination with serum-free medium.

Thus, the proteomic analysis was carried out and after data transformation, as described in paragraph 2.7.1, clusters were constructed and the resulting heatmap is shown in Fig. 4.

Samples SF18 and r-EPS 18 cluster with the controls (C) in the Ctrl cluster, indicating that these two treatments do not show relevant effects. Together with the control, they outline the basic cellular situation in the absence of treatments.

Another cluster (cluster 2) is formed by samples r-EPS 19 and PP19 with sample PP18, while sample SF19 stands alone (cluster 1). This suggests that the treatment with the soluble fraction of LB1932 strain has unique effects compared to the others. Biomarkers analyzed tend to organize in two large clusters (clusters A and B), showing an opposite behavior in samples clustered with or without controls. Within these two macro groups, some subgroups showed some differences between cluster 1 and cluster 2, as reported in Table S7.

Taking the Ctrl cluster as a reference, we observed that for both cluster 1 and cluster 2, proteins in cluster A are generally under-expressed (green), while those belonging to cluster B, are over-expressed (red). Considering the biomarkers involved in the proliferation process, we noted that in cluster A there is TNF-alpha, a mitogenic factor stimulating the proliferation of fibroblasts and the production of proteases [57], while in cluster B, the IL-1R-1 interleukins receptor [58] and PDGF subunit A, a powerful mitogen that favors fibroblasts proliferation by autocrine stimulation mechanism [57], are present. As for biomarkers involved in the extracellular matrix, cluster A contained the ECM degradation protein MMP3 [59,60] and the factor IGF1, which promotes cell growth and collagenase synthesis [58]; cluster B, on the
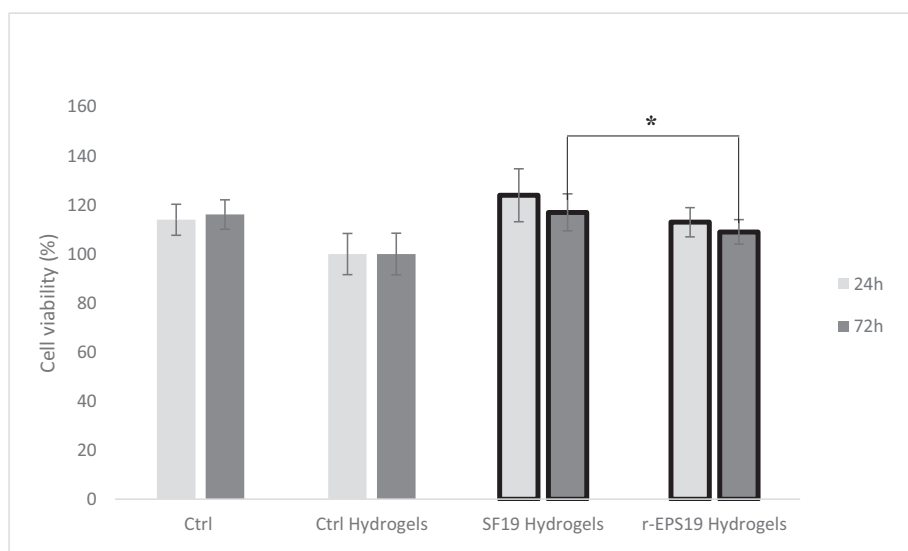
Fig. 3. Cell proliferation test with hydrogels. Cell viability for incubated samples with SF19 and r-EPS19 functionalized hydrogels is expressed as a percentage with respect to the mean of the control samples (Ctrl hydrogels, untreated); the results are reported as mean ± standard deviation of four independent measurements; results obtained for cells grown on nude plate (Ctrl) are also reported. Statistically significant differences ($p < 0.05$, T-student test) between Ctrl scaffolds are outlined in black, while asterisk (*) denotes the statistically significant difference (p < 0.05, T-student test) between functionalized hydrogels at 72 h.
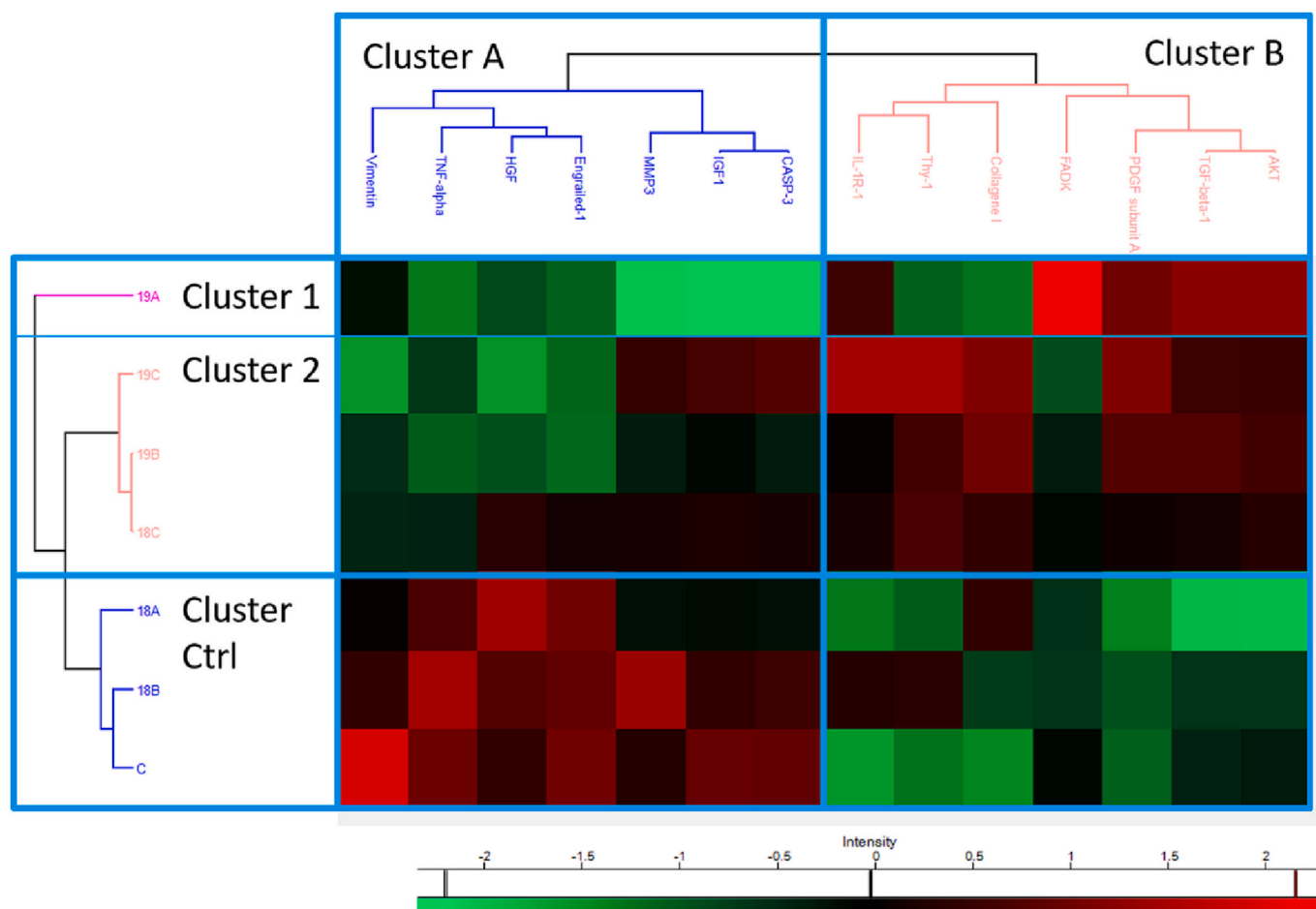
Fig. 4. Heatmap derived from data clustering on protein abundance derived from LC-MS / MS SRM analysis. Sample clusters: Cluster 1 (19A), Cluster 2 (19C, 19B, 18C), Cluster Ctrl (18A, 18B, C). Protein biomarkers clusters: Cluster A (Vimentin, TNF-alpha, HFF, Engrailed-1, MMP3, IGF1, CASP-3), Cluster B (IL-1R-1, Thy-1, Collagen I, FADK, PDGF subunit-I, TGF-beta-1, AKT). Downregulated proteins are represented in green, upregulated ones in red.

other hand, included collagen I, ECM components produced by fibroblasts [61], and the TGF-beta-1 factor, which stimulates chemotaxis and proliferation of fibroblasts as well as the deposition of collagen [58]. All the factors involved in the healing process such as HGF that accelerates re-epithelialization once secreted by fibroblasts [60], vimentin that is involved in feral healing [62] and Engrailed-1 which is associated with scars formation [63], are present in the cluster A. As regards apoptotic process biomarkers, cluster A contained only the proapoptotic factor CASP-3, while cluster B included the proapoptotic factor Thy-1 and the antiapoptotic factors AKT and FAK [64,65]. Therefore, treatment clusters (clusters 1 and 2) compared to the control cluster (cluster Ctrl) showed a reduction expression of proteins associated with ECM degradation (MMP3 and IGF1), proapoptotic factors (CASP-3) and biomarkers associated with the healing process (HGF, vimentin and Engrailed-1), and an increase in expression of proteins involved in ECM deposition (collagen I and TGF-beta-1) and in apoptosis process (Thy-1, AKT and FAK), of which the majority (AKT and FAK) have anti-apoptotic significance. Treatment clusters also appear to be characterized by an increase in two proliferative factors (IL-1R-1 and PDGF subunit A) compared to a decrease in the third factor considered for this category (TNF-alpha). These differences largely coincide with the divergence in behavior between samples LB18 and LB19. The only exception is constituted by sample 18C, which was included in cluster 2. Focusing on the differences between cluster 1 and cluster 2, FADK subgroup was weakly under expressed in cluster 2 and strongly over expressed in cluster 1, while CASP-3 subgroup was strongly over expressed in cluster 1 but weakly under expressed in cluster 2. Cluster 1 was further characterized by a

weak under-expression of Thy-1 and Collagen I and a weak over-expression of vimentin and AKT. This suggests an accentuation of the trend just described for the treatments (cluster 1 and 2) compared to cluster Ctrl, with intensified anti-apoptotic effect. In cluster 1 a decrease in collagen deposition could be probably associated with the increased IGF1 and MMP3 expression. A slight increase in vimentin expression, compared to cluster 2, together with the slight increase in TGF-beta-1 expression and the strong FAK increase, could suggest an augmented tendency to cell migration, with a possible regenerative significance.

Therefore, overall, these findings confirmed the difference in behavior between treatments derived from LB1865 and LB1932 strains. The derivatives of LB18, in fact, (except 18C) clustered with controls, and showed, compared to LB19 derivatives, an upregulation of factors involved in the degradation of the ECM, the proapoptotic factor CASP-3 and of factors associated with healing and scar formation, included in cluster A. Moreover, the downregulation of factors involved in the deposition of the ECM, antiapoptotic factors and factors associated with cell adhesion and migration processes, included in cluster B were observed for LB18 derivatives. The distribution of biomarkers associated with the proliferation process between clusters A and B, the first being upregulated and the second downregulated in the Ctrl cluster, suggests an overall balance of their effects and can explain the absence of substantial differences in viability detected by resazurin assay at 24 and 72 h. The derivatives of strain LB1932, on the other hand, outline an opposite situation compared to that described for those of LB1865, suggesting a generally favored antiapoptotic molecular structure, predisposed to ECM deposition and cell migration. These results confirmed

the choice of samples FS19 and r-EPS 19 as the most suitable for stimulating the regenerative effects observed in the scratch test.

4. Conclusions

The potential use of *L. bulgaricus* derivatives, characterized in terms of proteins, lipids, and EPS composition, in wound healing applications has been successfully investigated. LB derivatives extracted from two strains, LB1865 and LB1932, and suitably dosed after cytotoxicity studies, were used to formulate and manufacture, ALG and ALG/HA acid self-cross-linking 3D printed hydrogels as novel active dressing able to promote in-vitro fibroblast proliferation and migration. Our tests highlighted differences between the two strains' derivatives. In particular, the proteins of the soluble fraction and the r-EPS derived from LB1932 strain were able to stimulate cell migration with an increase of regenerative potential ranging from 10 to 20 %. This evidence was explained at the molecular level by a decrease in matrix-degrading and proapoptotic proteins, associated with an increase in collagen and anti-apoptotic proteins production. In the specific case of SF19 treatments, these effects seemed to be accentuated, associated with a decrease in collagen deposition and an increase in factors involved in cell migration. All these findings suggest a potential use of LB derivatives, such as proteins and EPS, embedded in 3D-printed hydrogels as advanced therapeutic solutions for successful applications in regenerative medicine, laying the basis for future investigations on this topic. In the view for future applications, this study could be implemented by deeply understanding the role of EPS and protein interactions in solution and on cell behavior; the setting of the LB derivatives concentrations tested in vitro on fibroblasts cells could also be implemented with studies in 3D in-vitro systems or in vivo. The optimization of the 3D printing parameters, which are set on the basis of the in house-build printer used, together with the exploration of other biomaterials to obtained hydrogels or even formulated as nanoparticles or films could be even explored. It is opinion of the Authors that a deeper investigation especially focused on the characterization of EPS produced by these different LB strains could allow to add significative insights into their biological properties and potential use, including antimicrobial, anti-inflammatory, antioxidant activities and personalized dosages.

CRediT authorship contribution statement

Giulia Remaggi: investigation, methodology, data curation, writing - original draft. **Benedetta Bottari:** supervision; writing, reviewing, and editing. **Elena Bancalari**: investigation, data curation, reviewing and editing. **Ovidio Catanzano:** methodology, writing - reviewing and editing. **Erasmo Neviani:** critical reviewing and supervision. **Lisa Elviri:** conceptualization, methodology, funding acquisition; project administration; supervision; writing - reviewing and editing.

Funding

Declaration of competing interest

X The authors declare that they have no known competing financial interests or personal relationships that could have appeared to influence the work reported in this paper.

Acknowledgments

Appendix A. Supplementary data

Supplementary data to this article can be found online at https://doi.org/10.1016/j.ijbiomac.2023.124454.

References

[1] A. Eltom, G. Zhong, A. Muhammad, Scaffold techniques and designs in tissue engineering functions and purposes: a review, Adv. Mater. Sci. Eng. 2019 (2019) 1–13, https://doi.org/10.1155/2019/3429527.

[2] C. Bergonzi, G. Remaggi, C. Graiff, L. Bergamonti, M. Potenza, M.C. Ossiprandi, I. Zanotti, F. Bernini, R. Bettini, L. Elviri, Three-dimensional (3D) printed silver nanoparticles/alginate/nanocrystalline cellulose hydrogels: study of the antimicrobial and cytotoxicity efficacy, Nanomaterials. 10 (2020) 844, https://doi.org/10.3390/nano10050844.

[3] G.C. Gurtner, S. Werner, Y. Barrandon, M.T. Longaker, Wound repair and regeneration, Nature 453 (2008) 314–321, https://doi.org/10.1038/nature07039.

[4] J. Boateng, O. Catanzano, Advanced therapeutic dressings for effective wound healing—a review, J. Pharm. Sci. 104 (2015) 3653–3680, https://doi.org/10.1002/jps.24610.

[5] T.R. Johnson, B.I. Gómez, M.K. McIntyre, M.A. Dubick, R.J. Christy, S.E. Nicholson, D.M. Burmeister, The cutaneous microbiome and wounds: new molecular targets to promote wound healing, Int. J. Mol. Sci. 19 (2018) 2699, https://doi.org/10.3390/ijms19092699.

[6] A. Sinha, S. Sagar, MM, W.Jabez Osborne, Probiotic bacteria in wound healing; an in-vivo study, Iran, J. Biotechnol. 17 (2019), e2188, https://doi.org/10.30498/IJB.2019.85188.

[7] R. Knackstedt, T. Knackstedt, J. Gatherwright, The role of topical probiotics on wound healing: a review of animal and human studies, Int. Wound J. 17 (2020) 1687–1694, https://doi.org/10.1111/iwj.13451.

[8] M. Mohtashami, M. Mohamadi, M. Azimi-Nezhad, J. Saeidi, F.F. Nia, A. Ghasemi, Lactobacillus bulgaricus and Lactobacillus plantarum improve diabetic wound healing through modulating inflammatory factors, Biotechnol. Appl. Biochem. n/a (n.d.). https://doi.org/10.1002/bab.2064.

[9] S. Fijan, A. Frauwallner, T. Langerholc, B. Krebs, J.A. ter Haar, A. Heschl, D. Mičetić Turk, I. Rogelj, Efficacy of using probiotics with antagonistic activity against pathogens of wound infections: an integrative review of literature, BioMed Res. Int. 2019 (2019) 7585486, https://doi.org/10.1155/2019/7585486.

[10] H. Chen, Y. Guo, Z. Zhang, W. Mao, C. Shen, W. Xiong, Y. Yao, X. Zhao, Y. Hu, Z. Zou, J. Wu, Symbiotic algae-bacteria dressing for producing hydrogen to accelerate diabetic wound healing, Nano Lett. 22 (2022) 229–237, https://doi.org/10.1021/acs.nanolett.1c03693.

[11] L. Mei, D. Zhang, H. Shao, Y. Hao, T. Zhang, W. Zheng, Y. Ji, P. Ling, Y. Lu, Q. Zhou, Injectable and self-healing probiotics-loaded hydrogel for promoting superbacteria-infected wound healing, ACS Appl. Mater. Interfaces 14 (2022) 20538–20550, https://doi.org/10.1021/acsami.1c23713.

[12] X. Tang, J. Zhao, Commercial Strains of Lactic Acid Bacteria with Health Benefits, in: W. Chen (Ed.), Lact, Acid Bact., Springer Singapore, Singapore, 2019, pp. 297–369, https://doi.org/10.1007/978-981-13-7832-4_10.

[13] A. Piccioni, L. Franza, V. Vaccaro, A. Saviano, C. Zanza, M. Candelli, M. Covino, F. Franceschi, V. Ojetti, Microbiota and probiotics: the role of limosilactobacillus reuteri in diverticulitis, Medicina (Mex.) 57 (2021) 802, https://doi.org/10.3390/medicina57080802.

[14] Update of the list of QPS-recommended biological agents intentionally added to food or feed as notified to EFSA 14: suitability of taxonomic units notified to EFSA until March 2021 | EFSA, (n.d.). https://www.efsa.europa.eu/en/efsajournal/pub/6689 (accessed November 9, 2022).

[15] G.M. Daba, M.O. Elnahas, W.A. Elkhateeb, Contributions of exopolysaccharides from lactic acid bacteria as biotechnological tools in food, pharmaceutical, and medical applications, Int. J. Biol. Macromol. 173 (2021) 79–89, https://doi.org/10.1016/j.ijbiomac.2021.01.110.

[16] F. Lombardi, P. Palumbo, A. Mattei, F.R. Augello, M.G. Cifone, M. Giuliani, B. Cinque, Soluble fraction from lysates of selected probiotic strains differently influences re-epithelialization of HaCaT scratched monolayer through a mechanism involving nitric oxide synthase 2, Biomolecules 9 (2019) 756, https://doi.org/10.3390/biom9120756.

[17] M. Shirzad, J. Hamedi, E. Motevaseli, M.H. Modarressi, Anti-elastase and anti-collagenase potential of lactobacilli exopolysaccharides on human fibroblast, Artif. Cells Nanomed.Biotechnol. 46 (2018) 1051–1061, https://doi.org/10.1080/21691401.2018.1443274.

[18] A.-V. Do, B. Khorsand, S.M. Geary, A.K. Salem, 3D printing of scaffolds for tissue regeneration applications, Adv. Healthc. Mater. 4 (2015) 1742–1762, https://doi.org/10.1002/adhm.201500168.

[19] M.A. Azad, D. Olawuni, G. Kimbell, A.Z.M. Badruddoza, Md.S. Hossain, T. Sultana, Polymers for extrusion-based 3D printing of pharmaceuticals: a holistic materials-process perspective, Pharmaceutics 12 (2020) 124, https://doi.org/10.3390/pharmaceutics12020124.

[20] D. Singh, A. Tripathi, S. Zo, D. Singh, S.S. Han, Synthesis of composite gelatin-hyaluronic acid-alginate porous scaffold and evaluation for in vitro stem cell growth and in vivo tissue integration, Colloids Surf. B Biointerfaces 116 (2014) 502–509, https://doi.org/10.1016/j.colsurfb.2014.01.049.

[21] Z. Jiang, B. Diggle, M.L. Tan, J. Viktorova, C.W. Bennett, L.A. Connal, Extrusion 3D printing of polymeric materials with advanced properties, Adv. Sci. 7 (2020) 2001379, https://doi.org/10.1002/advs.202001379.

[22] S. Jacob, A.B. Nair, V. Patel, J. Shah, 3D printing technologies: recent development and emerging applications in various drug delivery systems, AAPS PharmSciTech 21 (2020) 220, https://doi.org/10.1208/s12249-020-01771-4.

[23] S. Kotta, A. Nair, N. Alsabeelah, 3D printing technology in drug delivery: recent progress and application, Curr. Pharm. Des. 24 (2018) 5039–5048, https://doi.org/10.2174/1381612825666181206123828.

[24] P. Sánchez-Cid, M. Jiménez-Rosado, A. Romero, V. Pérez-Puyana, Novel trends in hydrogel development for biomedical applications: a review, Polymers 14 (2022) 3023, https://doi.org/10.3390/polym14153023.

[25] M. Abazari, T. Akbari, M. Hasani, E. Sharifikolouei, M. Raoufi, A. Foroumadi, M. Sharifzadeh, L. Firoozpour, M. Khoobi, Polysaccharide-based hydrogels containing herbal extracts for wound healing applications, Carbohydr. Polym. 294 (2022) 119808, https://doi.org/10.1016/j.carbpol.2022.119808.

[26] Advanced 3D-Printing Bioinks for Articular Cartilage Repair, (n.d.). https://ijb.whioce.com/index.php/int-j-bioprinting/article/view/511 (accessed October 17, 2022).

[27] A. Fatimi, O.V. Okoro, D. Podstawczyk, J. Siminska-Stanny, A. Shavandi, Natural hydrogel-based bio-inks for 3D bioprinting in tissue engineering: a review, Gels Basel Switz. 8 (2022) 179, https://doi.org/10.3390/gels8030179.

[28] F.J. O'Brien, Biomaterials & scaffolds for tissue engineering, Mater. Today 14 (2011) 88–95, https://doi.org/10.1016/S1369-7021(11)70058-X.

[29] L.F. Santos, I.J. Correia, A.S. Silva, J.F. Mano, Biomaterials for drug delivery patches, Eur. J. Pharm. Sci. 118 (2018) 49–66, https://doi.org/10.1016/j.ejps.2018.03.020.

[30] R. Ahmad Raus, W.M.F. Wan Nawawi, R.R. Nasaruddin, Alginate and alginate composites for biomedical applications, AsianJ. Pharm. Sci. 16 (2021) 280–306, https://doi.org/10.1016/j.ajps.2020.10.001.

[31] O. Catanzano, V. D'Esposito, S. Acierno, M.R. Ambrosio, C. De Caro, C. Avagliano, P. Russo, R. Russo, A. Miro, F. Ungaro, A. Calignano, P. Formisano, F. Quaglia, Alginate–hyaluronan composite hydrogels accelerate wound healing process, Carbohydr. Polym. 131 (2015) 407–414, https://doi.org/10.1016/j.carbpol.2015.05.081.

[32] O. Catanzano, V. D'Esposito, P. Formisano, J.S. Boateng, F. Quaglia, Composite alginate-hyaluronan sponges for the delivery of tranexamic acid in postextractive alveolar wounds, J. Pharm. Sci. 107 (2018) 654–661, https://doi.org/10.1016/j.xphs.2017.09.026.

[33] G. Remaggi, O. Catanzano, F. Quaglia, L. Elviri, Alginate self-crosslinking ink for 3D extrusion-based cryoprinting and application for epirubicin-HCl delivery on MCF-7 cells, Molecules 27 (2022) 882, https://doi.org/10.3390/molecules27030882.

[34] P. Rastogi, B. Kandasubramanian, Review of alginate-based hydrogel bioprinting for application in tissue engineering, Biofabrication 11 (2019), 042001, https://doi.org/10.1088/1758-5090/ab331e.

[35] J. Baier Leach, K.A. Bivens, C.W. Patrick Jr., C.E. Schmidt, Photocrosslinked hyaluronic acid hydrogels: natural, biodegradable tissue engineering scaffolds, Biotechnol. Bioeng. 82 (2003) 578–589, https://doi.org/10.1002/bit.10605.

[36] F. Zamboni, I.F. Cengiz, A.M. Barbosa, A.G. Castro, R.L. Reis, J.M. Oliveira, M. N. Collins, Towards the development of a female animal model of T1DM using hyaluronic acid nanocoated cell transplantation: refinements and considerations for future protocols, Pharmaceutics 13 (2021) 1925, https://doi.org/10.3390/pharmaceutics13111925.

[37] C. Winters, F. Zamboni, A. Beaucamp, M. Culebras, M.N. Collins, Synthesis of conductive polymeric nanoparticles with hyaluronic acid based bioactive stabilizers for biomedical applications, Mater. Today Chem. 25 (2022) 100969, https://doi.org/10.1016/j.mtchem.2022.100969.

[38] M. David-Raoudi, F. Tranchepain, B. Deschrevel, J.-C. Vincent, P. Bogdanowicz, K. Boumediene, J.-P. Pujol, Differential effects of hyaluronan and its fragments on fibroblasts: relation to wound healing, Wound Repair Regen. 16 (2008) 274–287, https://doi.org/10.1111/j.1524-475X.2007.00342.x.

[39] D.C. West, I.N. Hampson, F. Arnold, S. Kumar, Angiogenesis induced by degradation products of hyaluronic acid, Science 228 (1985) 1324–1326, https://doi.org/10.1126/science.2408340.

[40] E.G. Bligh, W.J. Dyer, A rapid method of total lipid extraction and purification, Can. J. Biochem. Physiol. 37 (1959) 911–917, https://doi.org/10.1139/o59-099.

[41] K. Wang, W. Li, X. Rui, X. Chen, M. Jiang, M. Dong, Characterization of a novel exopolysaccharide with antitumor activity from lactobacillus plantarum 70810, Int. J. Biol. Macromol. 63 (2014) 133–139, https://doi.org/10.1016/j.ijbiomac.2013.10.036.

[42] L. Elviri, R. Foresti, C. Bergonzi, F. Zimetti, C. Marchi, A. Bianchera, F. Bernini, M. Silvestri, R. Bettini, Highly defined 3D printed chitosan scaffolds featuring improved cell growth, Biomed. Mater. 12 (2017), 045009, https://doi.org/10.1088/1748-605X/aa7692.

[43] E. Bancalari, M. Gatti, B. Bottari, D. Mora, S. Arioli, Disclosing lactobacillus delbrueckii subsp. Bulgaricus intraspecific diversity in exopolysaccharides production, Food Microbiol. 102 (2022) 103924, https://doi.org/10.1016/j.fm.2021.103924.

[44] C. Li, J.-L. Zhao, Y.-T. Wang, X. Han, N. Liu, Synthesis of cyclopropane fatty acid and its effect on freeze-drying survival of lactobacillus bulgaricus L2 at different growth conditions, World J. Microbiol. Biotechnol. 25 (2009) 1659–1665, https://doi.org/10.1007/s11274-009-0060-0.

[45] C. Sohlenkamp, K.A. Galindo-Lagunas, Z. Guan, P. Vinuesa, S. Robinson, J. Thomas-Oates, C.R.H. Raetz, O. Geiger, The lipid lysyl-phosphatidylglycerol is present in membranes of rhizobium tropici CIAT899 and confers increased resistance to polymyxin B under acidic growth conditions, Mol. Plant-Microbe Interactions® 20 (2007) 1421–1430, https://doi.org/10.1094/MPMI-20-11-1421.

[46] W. Tang, M. Dong, W. Wang, S. Han, X. Rui, X. Chen, M. Jiang, Q. Zhang, J. Wu, W. Li, Structural characterization and antioxidant property of released exopolysaccharides from lactobacillus delbrueckii ssp. Bulgaricus SRFM-1, Carbohydr. Polym. 173 (2017) 654–664, https://doi.org/10.1016/j.carbpol.2017.06.039.

[47] K. Draget, K. Ostgaard, O. Smidsrod, Alginate-based solid media for plant tissue culture, Appl. Microbiol. Biotechnol. 31 (1989), https://doi.org/10.1007/BF00252532.

[48] S. Oerther, H. Le Gall, E. Payan, F. Lapicque, N. Presle, P. Hubert, J. Dexheimer, P. Netter, Hyaluronate-alginate gel as a novel biomaterial: mechanical properties and formation mechanism, Biotechnol. Bioeng. 63 (1999) 206–215.

[49] A. Serafin, M. Culebras, M.N. Collins, Synthesis and evaluation of alginate, gelatin, and hyaluronic acid hybrid hydrogels for tissue engineering applications, Int. J. Biol. Macromol. 233 (2023), 123438, https://doi.org/10.1016/j.ijbiomac.2023.123438.

[50] F. Zamboni, C. Okoroafor, M.P. Ryan, J.T. Pembroke, M. Strozyk, M. Culebras, M. N. Collins, On the bacteriostatic activity of hyaluronic acid composite films, Carbohydr. Polym. 260 (2021), 117803, https://doi.org/10.1016/j.carbpol.2021.117803.

[51] F. Zamboni, C.K. Wong, M.N. Collins, Hyaluronic acid association with bacterial, fungal and viral infections: can hyaluronic acid be used as an antimicrobial polymer for biomedical and pharmaceutical applications? Bioact. Mater. 19 (2023) 458–473, https://doi.org/10.1016/j.bioactmat.2022.04.023.

[52] M. Hamidi, O.V. Okoro, P.B. Milan, M.R. Khalili, H. Samadian, L. Nie, A. Shavandi, Fungal exopolysaccharides: properties, sources, modifications, and biomedical applications, Carbohydr. Polym. 284 (2022), 119152, https://doi.org/10.1016/j.carbpol.2022.119152.

[53] C. He, H.-Y. Lin, C.-C. Wang, M. Zhang, Y.-Y. Lin, F.-Y. Huang, Y.-Z. Lin, G.-H. Tan, Exopolysaccharide from paecilomyces lilacinus modulates macrophage activities through the TLR4/NF-κB/MAPK pathway, Mol. Med. Rep. 20 (2019) 4943–4952, https://doi.org/10.3892/mmr.2019.10746.

[54] C.-C. Liang, A.Y. Park, J.-L. Guan, In vitro scratch assay: a convenient and inexpensive method for analysis of cell migration in vitro, Nat. Protoc. 2 (2007) 329–333, https://doi.org/10.1038/nprot.2007.30.

[55] B.I. Pinto, N.D. Cruz, O.R. Lujan, C.R. Propper, R.S. Kellar, In vitro scratch assay to demonstrate effects of arsenic on skin cell migratio, J. Vis. Exp. (2019), e58838, https://doi.org/10.3791/58838.

[56] I.S. Organizaton, ISO 10993-5:2009 Biological Evaluation of Medical Devices, Part 5: Tests for Citotoxicity, in Vitro Methods, 2009.

[57] J.N. Mansbridge, K. Liu, R.E. Pinney, R. Patch, A. Ratcliffe, G.K. Naughton, Growth factors secreted by fibroblasts: role in healing diabetic foot ulcers, diabetes, Obes. Metab. 1 (1999) 265–279, https://doi.org/10.1046/j.1463-1326.1999.00032.x.

[58] P. Rožman, Ž. Bolta, Use of platelet growth factors in treating wounds and soft-tissue injuries, Acta Dermatovenerol. Alp. Pannonica Adriat. 16 (2007) 156–165.

[59] D. Lindner, C. Zietsch, P.M. Becher, K. Schulze, H.-P. Schultheiss, C. Tschöpe, D. Westermann, Differential expression of matrix metalloproteases in human fibroblasts with different origins, Biochem. Res. Int. 2012 (2012) 1–10, https://doi.org/10.1155/2012/875742.

[60] R. Kalluri, M. Zeisberg, Fibroblasts in cancer, Nat. Rev. Cancer 6 (2006) 392–401, https://doi.org/10.1038/nrc1877.

[61] I.R. da Silva, M.V. da Silva, A.B. Peixoto, C.A.X. Carneiro, M.A. dos Reis, P. C. Furtado, B.R. Rodrigues, V. Rodrigues, D.B.R. Rodrigues, L.C.R.da C. Tiveron, In situ cytokine expression and morphometric evaluation of total collagen and collagens type I and type III in keloid scars, Mediators Inflamm. 2017 (2017) 1–11, https://doi.org/10.1155/2017/6573802.

[62] F. Cheng, Y. Shen, P. Mohanasundaram, M. Lindström, J. Ivaska, T. Ny, J. E. Eriksson, Vimentin coordinates fibroblast proliferation and keratinocyte differentiation in wound healing via TGF-β–Slug signaling, Proc. Natl. Acad. Sci. 113 (2016) E4320–E4327, https://doi.org/10.1073/pnas.1519197113.

[63] S. Mascharak, M.F. Davitt, M. Griffin, M.R. Borrelli, A.L. Moore, K. Chen, B. Duoto, M. Chinta, D.S. Foster, A.H. Shen, M. Januszyk, S.H. Kwon, G. Wernig, D.C. Wan, H.P. Lorenz, G.C. Gurtner, M.T. Longaker, H.E. des Jardins-Park, Preventing engrailed-1 activation in fibroblasts yields wound regeneration without scarring, Science 372 (2021) eaba2374, https://doi.org/10.1126/science.aba2374.

[64] Controlling the Balance of Fibroblast Proliferation and Differentiation: Impact of Thy-1 | Elsevier Enhanced Reader, (n.d.). https://doi.org/10.1038/jid.2015.86.

[65] The mechanisms underlying fibroblast apoptosis regulated by growth factors during wound healing - Akasaka - 2010 - The Journal of Pathology - Wiley Online Library, (n.d.). https://onlinelibrary.wiley.com/doi/epdf/10.1002/path.2710 (accessed January 12, 2022).